



# Sensitivity assessment and lateral-torsional buckling design of I-beams using solid finite elements



Zdeněk Kala\*, Jan Valeš

Brno University of Technology, Faculty of Civil Engineering, Institute of Structural Mechanics, Veverí Street 95, 602 00 Brno, Czech Republic

## ARTICLE INFO

### Article history:

Received 28 October 2016

Received in revised form 5 September 2017

Accepted 10 September 2017

### Keywords:

Sensitivity analysis

Lateral-torsional buckling

Steel

Beam

Imperfections

Residual stress

## 1. Introduction

The ultimate load-carrying capacity (LCC) of a steel structure is the theoretical maximum load associated with the collapse of the structure. The high sensitivity of LCC to initial imperfections is inherent in all slender steel beams under compression or bending, which are subjected to loss of stability [1].

LCC is generally a random variable. The reliable design of slender steel structures requires the use of stochastic computational models as they take into consideration the random effects of all initial imperfections, including residual stresses. The random effects of initial imperfections on LCC may be studied using Monte Carlo (sampling based) approaches [2] in combination with the non-linear finite element method (FEM); it is a common approach in the simulation-based computational modelling of structural response [3,4].

The design LCC is the theoretical load that a steel structure can safely and reliably transfer while ensuring the probability of failure is small. The design LCC can be calculated according to the design philosophy of the relevant Eurocodes [5,6] and the reliability requirements in [7] as a quantile (percentile) of the LCC. The calculation procedures laid down in design standards [8] are calibrated so that their design values approximately correspond to the design quantiles specified in [7].

Data from experimental research concerning numerous material and geometric imperfections of steel structures are available for use with sto-

chastic computational models in the form of input random variables [9–12]. However, certain imperfections can only be measured experimentally with limited accuracy and their statistical characteristics are still under discussion. A typical example is residual stress, which can reduce LCC and thus increase the probability of structural failure [13,14]. The fundamental question is, how does the residual stress influence the random LCC in comparison to other imperfections? The answer can be obtained using appropriate methods of sensitivity analysis (SA); see reviews [15–19]. It is interesting that SA is used relatively less in the technical sciences than in scientific fields such as chemistry, medicine or biology [17].

SA methods are either deterministic or stochastic [20]. Stochastic SA methods are more relevant when sufficient data are available from experiments and accurate stochastic computational models [9,21]. On the other hand, deterministic SA methods are more frequently applied in cases where input data uncertainty is not of a stochastic nature. Examples include sensitivity formulations for optimal structural design [22–24] or fuzzy multiple-criteria decision-making techniques and their applications in economics and engineering [25,26].

Sensitivity analysis methods can generally be classified into local and global methods [15]. Local or one-factor-at-a-time methods are limited to examining the effects of variations in input parameters in the vicinity of their nominal values. Global SA methods define the contribution of individual input parameters, including their sets, and provide more comprehensive information on the computational model regarding changes in input parameters throughout their domain [27]. A wide range of global SA methods exists in all those situations where it is possible to assign probability distributions to model inputs [16]. Global SA techniques do not require a priori information on the nature of the model (model-free setting) because the conditions of additivity or linearity are not required [15]. The disadvantage of global SA methods is that they usually lead to computationally expensive estimates [28], while local SA methods require fewer simulation runs of the computational model [29].

If the output of the reliability analysis is a failure probability, SA can be applied based on the partial derivative of that failure probability with respect to the parameters of the input probability density functions (pdf) [30,31]. This type of SA is local, because the emphasis is on the local (point) effect of input factors on the model output. It usually requires repeated evaluation of the failure probability for different pdf parameters. If the limit state function is linear, first-order derivatives provide all the information needed for SA; see e.g [32]. However, in the case of non-linear limit state functions, this SA provides an approximate result with unknown precision [31].

\* Corresponding author.

E-mail addresses: kala.z@fce.vutbr.cz (Z. Kala), vales.j@fce.vutbr.cz (J. Valeš).

The subject of this article is the statistical and sensitivity analysis of the ultimate limit state of an imperfect steel I-beam which is subjected to lateral-torsional buckling. The reliability of the design procedure according to [8] is verified via the 0.1 percentile of LCC ( $LCC_{0.1}$ ), which is the design quantile defined for the target reliability index  $\beta_d = 3.8$  in [7]. The LCC is determined using geometric and material non-linear FEM analysis. Statistical and sensitivity analyses are performed using polynomial approximation of the LCC.

The statistical analysis takes into account the random nature of input imperfections and examines the randomness of LCC, where the key output is  $LCC_{0.1}$ . The goal of the SA is to describe the non-linear and non-additive relationships between the input factors and  $LCC_{0.1}$ . To that end, global SA based on two-level factorial design (FD) is employed. FD is the strategy of creating combinations of input factors for the design and implementation of physical or simulated experiments [33]. The effects on the model output are examined by altering the input factors. SA based on FD (SAFD) ranks these effects in order of importance from the most to the least significant. Mean values and standard deviations, which are the most commonly used parameters of the pdfs (usually Gauss) of input random variables of stochastic computational models (see for instance [34–36]), are selected as the factors of initial imperfections. The objective of SAFD is to examine the effects of these factors on  $LCC_{0.1}$ .

SAFD is performed within a deterministic framework, i.e., probability distributions are not assigned to the model inputs. SAFD deals with the “second degree of uncertainty” [37], where uncertainties (inaccuracies) in the statistic moments of input random imperfections are considered and the effects of such uncertainties on  $LCC_{0.1}$  are studied. The second degree of uncertainty is present wherever a component of the stochastic model (reliability system) is represented by knowledge-based (subjective) probability [37,38]. The introduction of two degrees of uncertainty has its justification. The first degree of uncertainty is dealt with via the statistical analysis of the LCC and quantified by calculating  $LCC_{0.1}$ . However, the authors sense that the value of  $LCC_{0.1}$  is influenced by (in addition to the random factors) other factors, the influence of which should be monitored. The objective of this paper is the analysis of the second degree of uncertainty of  $LCC_{0.1}$  using global SAFD and an advanced geometric and material non-linear FE model.

The purpose of the current study, which differs from that of the recent study [39] performed by the authors on a similar topic, is the statistical and global sensitivity analysis of  $LCC_{0.1}$ . The application of Sobol's sensitivity analysis with regard to LCC was described in [39] but is not the subject of the current study. This study and [39] have some overlap with regard to the non-linear FE model and its random imperfections, but the performance of different sensitivity assessments and a new statistical analysis of reliability with consideration given to Eurocode 3 rules are described in this current article.

## 2. Finite element model

The research is focused on the ultimate limit state of a European double symmetric hot-rolled beam (IPN 200), see Fig. 1. The I-beam is subjected to lateral-torsional buckling due to uniform bending moment  $M$ , see Fig. 2. The goal of the non-linear finite element analysis is to quantify the effects of initial imperfections on the LCC of the beam. The LCC is analysed using the ANSYS software package, which provides sophisticated solid finite element analyses (FEA) using non-linear constitutive laws and adopting incremental-iterative techniques [39]. The model has been developed using the 8-node homogeneous structural solid element SOLID185; it is suitable for studying large deflections, large strain capabilities, plasticity, hyper-elasticity, stress stiffening and creep [40]. The finite element model (FEM) based on SOLID185 elements includes geometric and material non-linearities. The enhanced strain formulation is considered.

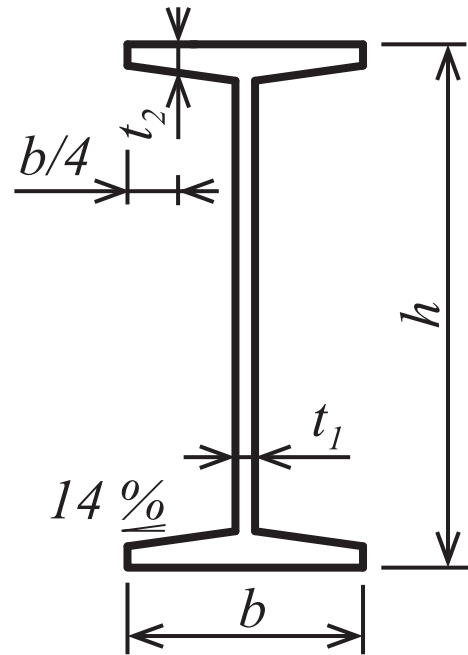


Fig. 1. The geometry of an IPN 200 beam.

### 2.1. Mesh, boundary conditions and loads

The model of the IPN 200 cross-section is defined using a closed 2D polygonal line that encloses a biaxially symmetrical geometric shape (idealized cross-section) with the dimensions  $h$ ,  $b$ ,  $t_1$  and  $t_2$ , see Fig. 1. The idealized cross-section neglects the fillets at the ends of the flanges and at the transitions between the web and the flanges, thus eliminating possible problems with the discretization of the model using finite element meshes.

Several finite element mesh creation variants with different settings for the number of elements were compared in order to find a compromise between CPU time consumption and the accuracy of results. The optimum mesh is generated using ten elements for the flange width, twenty elements for the web height and two elements for the thickness of the web and flange; see Fig. 3.

Translations  $u_x$ ,  $u_y$ ,  $u_z$  and rotations  $\varphi_x$ ,  $\varphi_y$ ,  $\varphi_z$  relate to the global Cartesian coordinate system, which has its origin at the end of the beam in the centre of gravity. The  $x$ -axis is the longitudinal axis of the beam prior to the introduction of bow imperfection, while the  $y$  and  $z$ -axes lie in the plane of the section. The number of elements in the direction of the  $x$ -axis increases as the beam length increases. The condition that the ratio of the longest to the shortest side of the element must be  $< 8$  must be fulfilled. Let us note that according to [40], the aspect ratio for quadrilaterals should not exceed 20 or the analysis results may be adversely affected.

End-fork boundary conditions were assumed for the model. Such boundary conditions are created using three kinematic coupling constraints [4], see Fig. 4. Two of these are added to the tips of the flanges

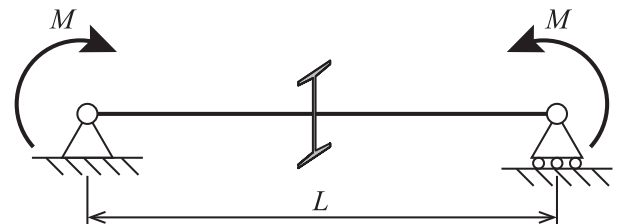


Fig. 2. Simply supported I-beam subjected to uniform bending moment.

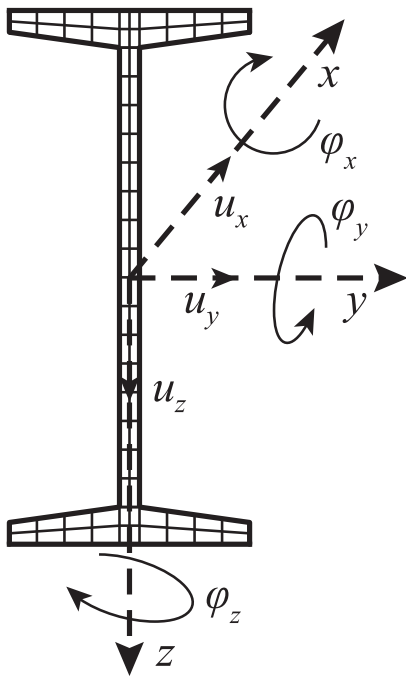


Fig. 3. The meshing of an IPN 200 cross-section.

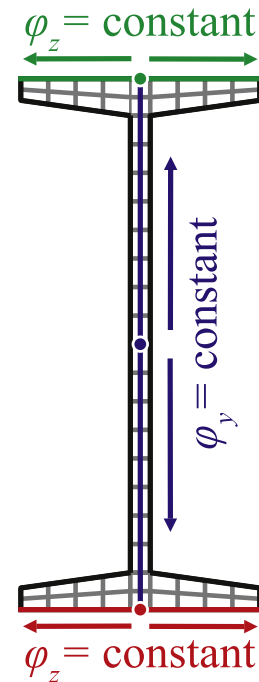


Fig. 4. Three kinematic coupling constraints.

and one is applied to the axis of the web. Each coupling constraint introduces a constant rotation along its lines. Kinematic coupling constraints are an important part of the model because they prevent local stress extremes from arising in the end sections, which is a problem that would otherwise occur due to the loading forces.

The beam model is loaded at both ends by equal pure bending moments  $M$ , see Fig. 2. The bending moments are applied as surface loads on the surface  $p$  [N/m<sup>2</sup>], whose distribution over the cross-section is of the same shape as the distribution of the normal stress from bending, see Fig. 5. The equation from the theory of elasticity of beams  $p = Mz/I_y$ , where  $I_y$  is the second moment of area about the  $y$ -axis, is applied.

The boundary conditions of both ends of the beam are introduced into the centre of gravity and  $u_y = u_z = \phi_x = 0$  is considered, see Fig. 5. The geometry, boundary conditions, loading and material properties of the model are symmetric about the plane at beam midspan, which is perpendicular to the  $x$ -axis. Translation in the direction of the  $x$ -axis is fixed at  $u_x = 0$  in the centre of gravity at beam midspan.

To ensure that the end-support conditions are modelled accurately, comparison of the elastic critical moment  $M_{cr-Ansys}$  (determined as an eigenvalue using the FE model) and  $M_{cr}$  (obtained from the beam theory [41]) is provided. Discrepancies in terms of the percentages  $(1 - M_{cr-Ansys}/M_{cr}) \cdot 100$  evaluated for 4 beams ( $L/h > 10$ ) are  $-6.58\%$  ( $L = 2.08$  m),  $-4.43\%$  ( $L = 3.49$  m),  $-1.96\%$  ( $L = 6.94$  m),  $0.46\%$  ( $L = 32.52$  m). The discrepancies in the percentages of slender beams are relatively small and show that the introduced boundary conditions model the fork-end support conditions at the supports with sufficient precision.

LCC is evaluated using the geometric and material non-linear FEM based on the incremental iterative strategy of the full Newton-Raphson method [40]. The external loading bending moment  $M$  increases step-by-step up to the LCC, for which the determinant of the tangential stiffness matrix of the beam is equal to zero. The LCC is numerically determined by the value of the external moment in the last loading step. The steps of the loading moment decrease so that the LCC value is calculated with an accuracy of 0.2%. The LCC calculated (i) using the increment of the external load is practically the

same as if it were calculated using (ii) the Riks arc-length method [42] because the stiffness matrix is positive definite during the entire process. Both methods can be used. It should be noted that the calculation performed in this article is based on the ultimate limit state, and no deflection limit was considered. Another method for obtaining the LCC is by applying deformation load when rotations about the  $y$ -axis are prescribed to the cross-section nodes on both ends [60]. In this case, a post-peak response can be observed and the peak load value is the LCC. The study in [60] has proved that LCCs obtained using both the deformation load and the force load are equal.

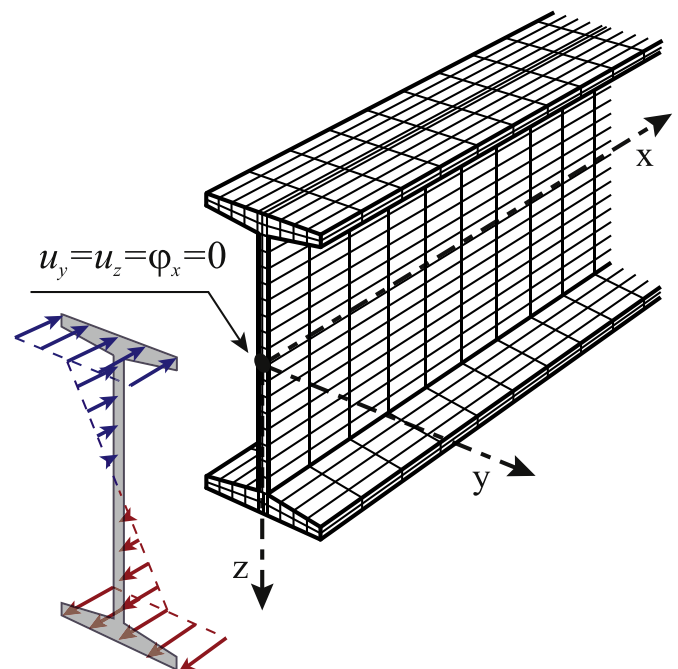


Fig. 5. End-fork boundary conditions and equal bending moments.

2.2. Material model

The relationship between the stress and strain is introduced as an elastic-plastic stress-strain bilinear diagram with an elastic part and pseudo-strain hardening. The elastic part with Young's modulus  $E$  is followed by a strain-hardening part with strain-hardening modulus  $E_{sh} = E/10000$ , where  $E_{sh}$  is the value taken from [43]. The inclusion of very small  $E_{sh}$  values helps overcome the numerical instability of the non-linear FEM model, which slightly increases when the value of the strain hardening exponent approaches zero. According to our studies, the influence of the size of strain-hardening on LCC is very small for beams under bending with small slenderness values. This is consistent with modelling the behaviour of compressed columns using shell elements [4]. It may be noted that a more sophisticated approach can be used to describe the stress-strain relationship. It involves using a trilinear diagram consisting of an elastic part and a yield plateau followed by a strain-hardening part, see e.g. [12,13,44].

2.3. Geometric imperfections

Geometric imperfections of the beam axis are taken into account in the shape of the first eigenmode, which is a common approach for introducing initial translations and rotations of a section along the length of a beam [44–48]. The first eigenmode is calculated on a perfectly straight beam (without imperfections), whose model is described above. Geometric imperfections based on this first eigenmode comprise lateral initial translation and initial rotation, both of which have a sinusoidal shape with the amplitudes  $a_{v0}$  and  $a_{\varphi0}$ , respectively.

$$v_0 = a_{v0} \sin\left(\frac{\pi x}{L}\right), \varphi_0 = a_{\varphi0} \sin\left(\frac{\pi x}{L}\right) \tag{1}$$

Both amplitudes  $a_{v0}$  and  $a_{\varphi0}$  can be expressed as functions of the initial bow imperfection  $e_0$ , which is located at the centre of the top flange edge at the midspan and is thus the most significant in terms of the size of the initial translation, see Fig. 6. Taking into account the analytical solution [41,49] or [50], we can write.

$$a_{v0} = \frac{e_0}{1 + \frac{h \pi^2 E I_z}{2 M_{cr} L^2}}, a_{\varphi0} = a_{v0} \frac{\pi^2 E I_z}{M_{cr} L^2} \tag{2}$$

where  $h$  is the cross-section height,  $L$  is the length of the beam,  $I_z$  is the second moment of area of the  $z$ -axis,  $E$  is Young's modulus and  $M_{cr}$  is the elastic critical moment when lateral beam buckling occurs, as described in [49,50].

2.4. Residual stress

One of the most challenging aspects of attempting the accurate FE analysis of the real behaviour of steel members is the modelling of residual stress. The distribution of residual stress in real steel members can only be obtained from experimental measurements. However, it is known to be a very difficult, time-consuming and inefficient task with limited accuracy [14]. The production of hot-rolled steel I-beams involves the cooling of the material into its final form, during which residual stresses arise primarily due to uneven cooling. The size and distribution of residual stress depend on the geometry and type of cross-section, rolling temperature, cooling conditions, straightening procedures and other factors. Results obtained from experimental research have demonstrated that the magnitude of residual stress in hot-rolled profiles appears to be independent of the material yield strength for both mild and high-strength steels [4]. The stress distribution ought to be independent of the yield stress. However, it does not have an effect on the analysis performed for S235 steel, which is used for the simulation. An entirely different situation is observed for welded beams, where residual stress in the vicinity of the welds can be as high as the yield strength [44,51]. The distribution of residual stress on the web and flanges of hot-rolled steel beams is well documented and can be idealized using a parabolic or linear curve [52]. The commonly used residual stress pattern for hot-rolled I-profiles in FE modelling is linear stress distribution, which is the basis for European buckling curves [53,4,54]. Linear distributions of residual stress can be used to determine accurate results which might be slightly more conservative than those obtained using a parabolic residual stress distribution [4].

The residual stress of the hot-rolled IPN 200 beam is introduced as thermal stress initiated by the application of temperature distributions to the web and flanges; it is the approach applied for rolled I-sections in similar studies, see e.g. [55,56,57,4]. If the flange has a rectangular cross-section as considered in, for instance [76,4], then the dependence between the residual stress and temperature change  $\Delta T$  is expressed by Eq. (3)

$$\Delta T = -\frac{\sigma_R}{E \cdot \beta} \tag{3}$$

where the temperature change  $\Delta T$  needed at a given point of the cross-section depends on the thermal expansion coefficient  $\beta = 1.2E - 5 \text{ K}^{-1}$  and the magnitude of the residual stress  $\sigma_R$  to be established at that point [57,4]. The effect of cold-straightening is neglected.

The residual stress is introduced with the use of thermal and structural analysis. The 3-D thermal solid element SOLID70 is used for the thermal analysis. SOLID70 only has a single degree of freedom, temperature, and cannot be used for stress state analysis. The output of the thermal analysis is a temperature field calculated from the required target temperatures in selected nodes. The temperature field

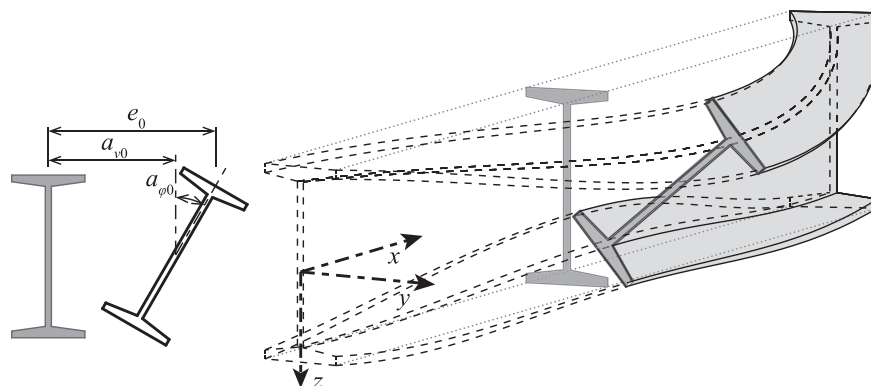


Fig. 6. Initial axis imperfection pattern based on the first eigenmode.

shown in Fig. 7 was created by entering target temperatures in selected nodes on the edges of the flanges, in the centre of the web and in the centre of the flange. In the next step, the element is changed to SOLID185. The distribution of residual stress is obtained by introducing the temperature field to the model with SOLID185 elements during the structural analysis, see Fig. 8. The equilibrium of forces in the direction of axis  $x$  is ensured automatically as the beam has a boundary condition,  $u_x = 0$ , in the centre of gravity in  $L/2$ .

However, since the flanges of the IPN cross-section have a 14% inclination angle towards the web, Eq. (3) has the nature of an approximate relation, which cannot be used directly. The introduction of self-equilibrating residual stresses is achieved by the FE analysis of the FE model described above.

Let us consider a fixed  $t_2$  value, see Fig. 1. The procedure for the introduction of the residual stress can be described as follows: Let us denote the value of the residual stress at the flange tips at any point at the midspan of the beam using variable  $\sigma_R$ . Temperature change  $\Delta T$ , which initiates the distribution of residual stress, is introduced in the computational model in the manner depicted in Fig. 7. For the fixed  $t_2$  value (i.e. fixed geometry) the obtained model dependence between residual stress and  $\Delta T$  is linear. The required residual stress value is obtained using new  $\Delta T$  settings; it is calculated as follows: the former  $\Delta T$  value obtained according to Eq. (3) is multiplied by the desired value  $\sigma_R$  and divided by the normal stress value  $\sigma_x$  from the FE model.

Fig. 7 and Fig. 8 show the relationship between the temperature distribution  $\Delta T$  and residual stress for nominal geometric characteristics  $h, b, t_1, t_2$ , where nominal flange thickness is  $t_2 = 11.3$  mm.

The residual stress introduced in such a manner changes almost linearly in the direction from the tips of the flange to its centre. It is 20% higher at the flange tips where the flange thickness is lower than at its centre, see Fig. 8. The zero stress value does not occur at the quarter of the way across the flange, but slightly closer to the centre. If we consider a rectangular flange shape, e.g. on an IPE profile, then the absolute residual stress values at the tips and centre of the flange are identical. The distribution of residual stress shown in Fig. 8 is one of the many possible types of self-equilibrating distribution. Other modelling approaches (e.g. parabolic distribution) can be discussed.

2.5. Validation of a solid FE model against a shell FE model

The above-described FE model (i) was validated using an FE model (ii) developed at the Technical University of Denmark [4,58]. Model (i) uses SOLID185 solid elements in ANSYS software [40], while model (ii) uses S4 shell elements in Abaqus software [59]. The calculation of

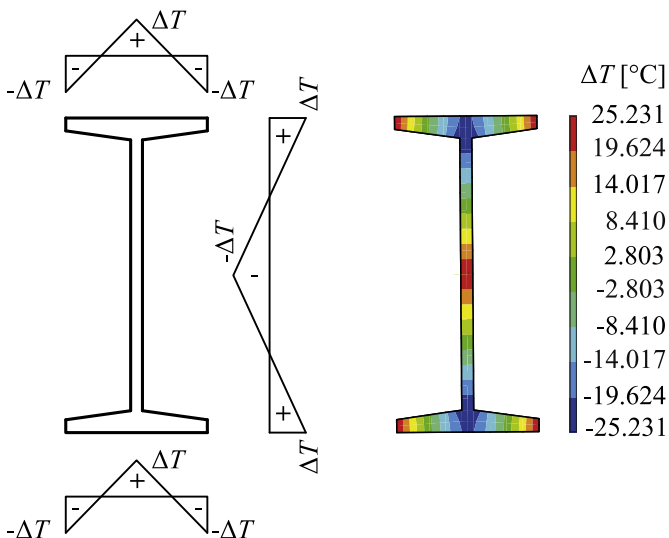


Fig. 7. Application of linear temperature changes  $\Delta T$  for the initiation of residual stress.

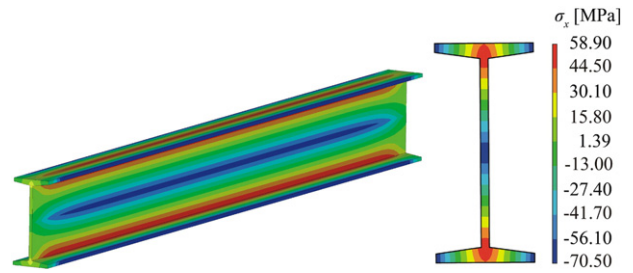


Fig. 8. Distribution of residual stress initiated by  $\Delta T$ .

the LCC for model (i) is based on the incremental iterative strategy of the Newton-Raphson method, and on the Riks arc-length method in the case of model (ii) [42]. Both FE models use the same material model, residual stress distribution and initial geometrical imperfections. Boundary conditions and loading are adapted to the elements used (solid in (i) and shell in (ii)). The validation of the LCC is performed with a series of IPE 200 beams. Analyses are performed for three values of  $\bar{\lambda}_{LT} = 0.3, 0.6$  and  $1.2$ . With 7 input random imperfections and 10 LHS runs, the standard deviations of the LCC of (i) are approximately 3–6% lower than those of (ii). The mean LCC values obtained from model

Run	Factor				
	A	B	C	D	E
1	–	–	–	–	–
2	+	–	–	–	–
3	–	+	–	–	–
4	+	+	–	–	–
5	–	–	+	–	–
6	+	–	+	–	–
7	–	+	+	–	–
8	+	+	+	–	–
9	–	–	–	+	–
10	+	–	–	+	–
11	–	+	–	+	–
12	+	+	–	+	–
13	–	–	+	+	–
14	+	–	+	+	–
15	–	+	+	+	–
16	+	+	+	+	–
17	–	–	–	–	+
18	+	–	–	–	+
19	–	+	–	–	+
20	+	+	–	–	+
21	–	–	+	–	+
22	+	–	+	–	+
23	–	+	+	–	+
24	+	+	+	–	+
25	–	–	–	+	+
26	+	–	–	+	+
27	–	+	–	+	+
28	+	+	–	+	+
29	–	–	+	+	+
30	+	–	+	+	+
31	–	+	+	+	+
32	+	+	+	+	+

Fig. 9. A  $2^k$  design for  $k = 1, 2, 3, 4$  and  $5$ .

(i) are lower than those from (ii) by approximately 2–6%. The difference of 6% occurs for  $\bar{\lambda}_{LT} = 0.3$ ; it may be induced by plastic behaviour in combination with the material overlap in model (ii). However, the crucial factor is the correlation between both models, which is almost 1 in each case. A detailed description of the comparative studies and obtained results is in [58].

In further comparative studies [60,61] the elastic resistance  $M_{R,Ansys}$  was validated using the analytical elastic solution  $M_R$  in the closed form [50].  $M_{R,Ansys}$  is calculated using model (i), where residual stress is neglected and material and geometric characteristics are considered using their nominal values.  $M_{R,Ansys}$  and  $M_R$  represent the bending moments at which the maximum value of the von Mises stress corresponds to yield strength. It is evident from [60,61] that  $M_{R,Ansys}$  perfectly corresponds to  $M_R$  for  $\bar{\lambda}_{LT}$  0 to 2.1.

**3. Factorial designs and sensitivity analysis**

Design of Experiments (DOE) is an important part of the planning and proposal of physical experiments [33]. The extension of DOE to computer experiments may be considered the predecessor of sensitivity analysis [15]. Although there are differences between physical and simulated experiments, sensitivity analysis (SA) is based on the same principles. SA evaluates the performance of a designed experiment, which is usually related to determining the effects of changed controllable inputs on the corresponding varied output of a process [62]. The combination of input factors (sample sets) should be chosen in such a manner so as to obtain the most relevant response function. The

**Table 1**  
Statistical characteristics of input imperfections.

Symbol	Characteristic	Pdf	Mean $\mu$	Standard deviation $\sigma$
$t_2$	Flange thickness	Gauss	11.3 mm	0.518 mm
$f_y$	Yield strength	Gauss	297.3 MPa	16.8 MPa
$E$	Modulus of elasticity	Gauss	210 GPa	10 GPa
$e_0$	Initial imperfection	Gauss	0	L/1960
res	Residual stress on flange tips	Gauss	90 MPa	18 MPa

sophisticated selection of combinations of input factors aimed at investigating the relationship between input-output was first proposed in [63]. A description of the classical design approach is published in, for example books [64,65]. An overview of other approaches to DOE can be found in, e.g [66–68].

A DOE technique with great practical significance is Factorial Design (FD) [15,33]. FD is the strategy of planning an experiment in such a manner that data are collected with the aim of determining the input factors and interactions between factors having the greatest influence on the response of the experiment [67]. FD assigns two levels to all factors, usually denoted by a high (+1 or simply +) and low (−1 or just −) level for each factor [64,67]. The FD is performed on all possible factor level combinations for all factors. The computational cost is  $n = 2^k$  runs, where  $k$  is the number of factors. The combinations of levels simulated in the design are displayed in a matrix referred to as the design matrix. The procedure of creating the factorial design matrix for three factors is published with supplementary illustrations in, e.g. [33,15]. A design matrix for four factors is published in [69–71], for example. An example of a design matrix for five input factors (A, B, C, D, E) is illustrated in Fig. 9. The subsets in Fig. 9 show how the number of combinations increases with an increasing number of factors  $k = 1, 2, 3, 4$  and 5.

The creation of  $2^5 = 32$  combinations of all levels can be written in the programming language Pascal as:

```
S:= ' - + ' ; For i1:=1 to 2 do For i2:=1 to 2 do For i3:=1 to 2 do
For i4:=1 to 2 do For i5:=1 to 2 do writeln(S[i5], S[i4], S[i3], S[i2], S[i1]);
```

(4)

Each combination yields an output,  $y_i$ . The design matrix extended by outputs  $y_i$  is used to evaluate the main and interaction effects of input factors on output  $Y$ . The difference between the output values  $y_1$  and  $y_2$  is solely due to variations at the level of variable  $A$ , since the other variables remain unchanged. Other differences in the output values relevant to the main effect of variable  $A$  exist between  $y_4$  and  $y_3$ ,  $y_6$  and  $y_5$ ,  $y_8$  and  $y_7$ , etc. The main effect of variable  $A$  is defined as the average effect of that variable over all conditions of other factors. For example, the main effect of variable  $A$  for three factors can be written as:

$$S_A = \frac{(y_2 - y_1) + (y_4 - y_3) + (y_6 - y_5) + (y_8 - y_7)}{4} \tag{5}$$

**Table 2**  
Artificial random variables for approximation.

Symbol	Characteristic	Pdf	Minimum	Maximum
$X_1$	Flange thickness	Rectangular	8.83 mm	13.77 mm
$X_2$	Yield strength	Rectangular	217.43 MPa	377.17 MPa
$X_3$	Modulus of elasticity	Rectangular	162.46 GPa	257.54 GPa
$X_4$	Initial imperfection	Rectangular	0	4.76 L/1960
$X_5$	Residual stress on flange tips	Rectangular	0 MPa	180 MPa

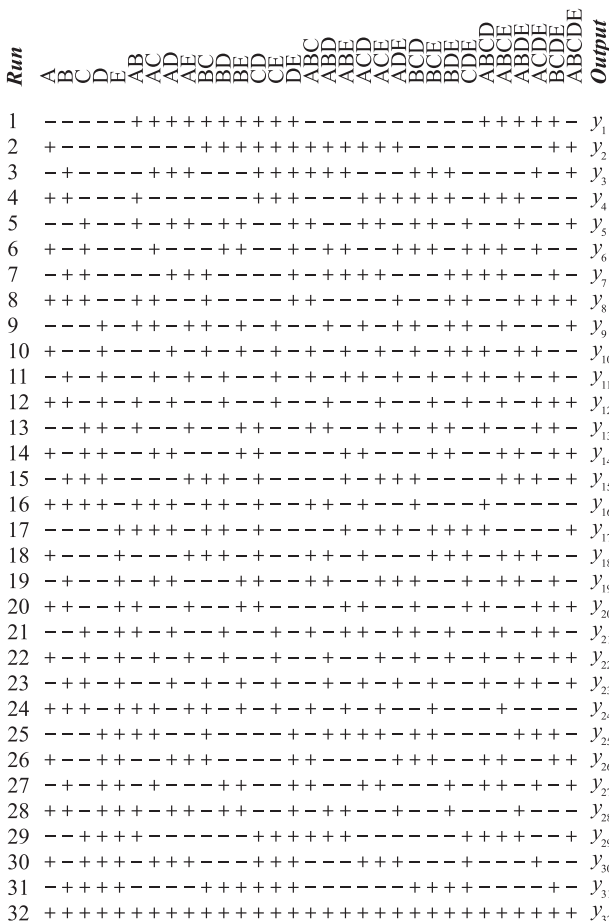


Fig. 10. Table of contrast coefficients  $c_{ij}$  for  $2^5$  design.

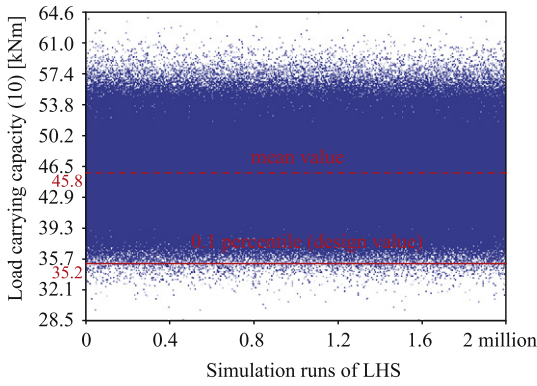


Fig. 11. Statistical analysis of LCC for  $\bar{\lambda}_{LT} = 1.0$  ( $L = 2.96$  m).

where  $S_A$  is the first order sensitivity index (main effect) of factor  $A$  on output  $Y$  [15]. The sensitivity index  $S_A$  for five factors can be written as:

$$S_A = \frac{1}{16} \sum_{i=1}^{16} (y_{2i} - y_{2i-1}) \quad (6)$$

The first order sensitivity index of factor  $B$  on output  $Y$  can be written analogously.

$$S_B = \frac{1}{8} \sum_{i=1}^8 (y_{4i-1} - y_{4i-3})(y_{4i} - y_{4i-2}) \quad (7)$$

The first order sensitivity indices of the other factors are calculated in a similar manner. Factorial design enables the measurement of interactions between each different group of factors. The interaction effects are calculated by extending the design matrix with a column containing contrast coefficients. The signs of the interactions are obtained by multiplying the signs of the respective variables; this is illustrated in Fig. 10 for 5 factors. Generally, the number of all sensitivity indices is  $2^k - 1$ .

For five input factors  $2^5 - 1 = 31$ , sensitivity indices exist, of which 5 describe the main effects,  $\binom{5}{2} = 10$  two-factor interactions,  $\binom{5}{3} = 10$  three-factor interactions,  $\binom{5}{4} = 5$  four-factor interactions, and one five-factor interaction. Using the table in Fig. 10, we can express the  $j$ -th sensitivity index as:

$$S_j = \frac{2}{n} \sum_{i=1}^n (c_{ij} y_i) \quad (8)$$

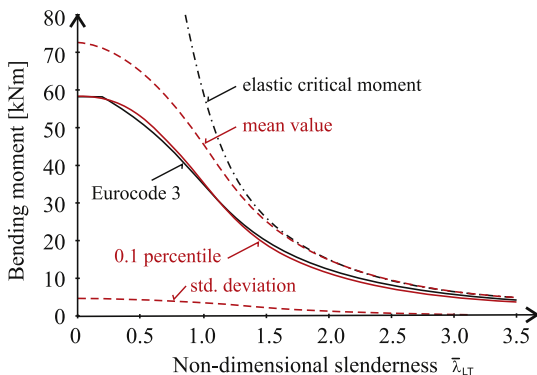


Fig. 12. Statistical analysis of LCC for pdfs from Table 1.

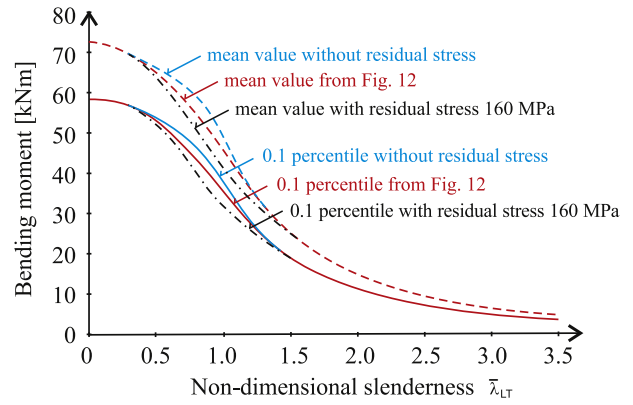


Fig. 13. Statistical analysis of LCC - residual stress.

where  $c_{ij}$  is the sign on the  $i$ -th row and  $j$ -th column and  $y_i$  is the output on the  $i$ -th row of the table in Fig. 10. For example, the interaction effect of factors  $A$  and  $B$  is calculated as

$$S_6 = S_{AB} = \frac{2}{32} (y_1 - y_2 - y_3 + y_4 + y_5 - y_6 - y_7 + \dots + y_{32}) \quad (9)$$

Sensitivity indices (Eq. (8)) may either be positive or negative. However, it is the mutual comparison of the absolute values of sensitivity indices that is significant for the interpretation of structural mechanics results.

SA based on FD (SAFD) has, in comparison with other methods, its advantages and disadvantages. SAFD can be used to examine the effects of deterministic (non-random) input factors of a stochastic computational model on changes in the statistical (moment or quantile) characteristics of output random variables [72]. One disadvantage is that a change in each input factor is expressed using only two values. This may be an advantage in cases where the uncertainties of input and output factors are expressed using fuzzy numbers and processed using the general extension principle based on  $\alpha$ -cuts [73].

#### 4. Input random imperfections

Stochastic models dealing with lateral-torsional buckling must include the effects of input material, geometric imperfections and residual stress. Random variability should be taken into account for those imperfections whose variability significantly influences the variability of the LCC. Stochastically significant imperfections include the initial curvature of the beam axis, flange thickness, yield strength, modulus of elasticity and residual stress. The significant effects of the first four imperfections

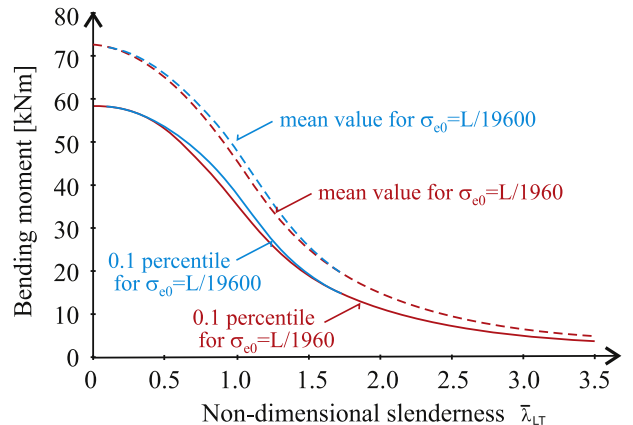


Fig. 14. Statistical analysis of LCC - bow imperfection.

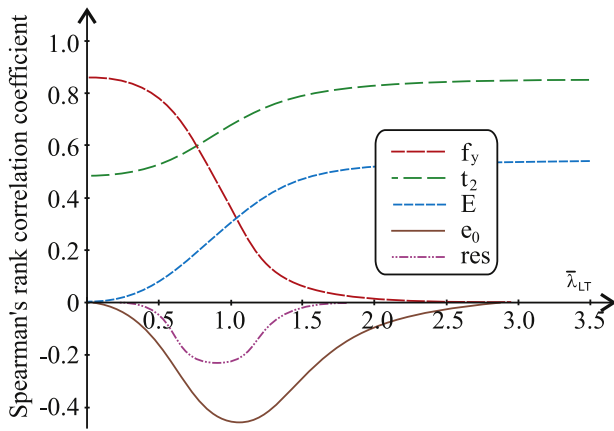


Fig. 15. Spearman rank-order correlation coefficients for imperfections vs LCC.

were confirmed by the SA of the elastic LCC [50]. It has also been observed that the random variabilities of the thickness of the web, the cross-section height, the thickness of the flange and Poisson's ratio do not significantly influence the elastic LCC and thus can be considered deterministic variables [50]. Residual stress in hot-rolled beams is another inevitable imperfection. It must be considered a random variable and its effect on LCC must be studied with regard to plasticity and instability effects [14].

The amplitude of the initial curvature of beam axis  $e_0$  is considered using a Gauss pdf. The mean value was considered to be zero, i.e., a perfectly straight beam (with simply supported ends) is introduced as the best representation of the mean value of all possible observations of the initial axial curvature. The magnitude of the beam bow imperfection can be taken as  $L/1000$ , [74,44,60]. The standard deviation  $L/1960$  is derived on the assumption that 95 observations (realizations) of amplitude  $e_0$  lie within the tolerance limits  $\pm L/1000$ , see e.g. [50,75].

The flange thickness  $t_2$  is modelled using a Gauss pdf with a mean value of 11.3 mm (nominal value) and a standard deviation of 0.518 mm [11]. Yield strength  $f_y$  is modelled using a Gauss pdf with a mean value of 297.3 MPa and a standard deviation of 16.8 MPa [9]. The statistical characteristics of the yield strength were evaluated from 562 tensile tests of samples obtained from a third of the flanges of profiles ranging from IPE 160 to IPE 220 [9]. The modulus of elasticity is modelled by a Gauss pdf with a mean value equal to the nominal value of 210 GPa and a standard deviation of 10 GPa [76].

An extensive literature survey [13] focused on probabilistic approaches to the modelling of the residual stress of hot-rolled steel I-sections shows the high random variability of experimentally observed magnitudes of residual stress. The residual stress  $res$  on the flange tips (see Fig. 8) can be modelled using a Gauss pdf with a mean value of 90 MPa and standard deviation of 18 MPa (coefficient of variation 0.2) [13].

All five input random variables are listed in Table 1. The variables in Table 1 are considered statistically independent. Other material and geometric characteristics are considered deterministic in the computational model. These include the nominal height ( $h = 200$  mm), nominal width ( $b = 90$  mm) and nominal web thickness ( $t_1 = 7.5$  mm) of a

European profile (IPN 200). Shear modulus is considered using the relation  $G = E/(2(1 + \nu))$ , where  $\nu$  is Poisson's ratio ( $\nu = 0.3$ ) [8].

## 5. Polynomial approximation of the load-carrying capacity

In order to reduce the computational cost of the structural reliability analysis, the non-linear response of the FE model is approximated by a polynomial (10), whose function values are easy to calculate. The terms of the polynomial are selected so as to approximate all non-linear and interaction effects of the five input variables on the output of the non-linear FE model.

$$LCC \approx Y = \sum_{a=0}^2 \sum_{b=0}^2 \sum_{c=0}^2 \sum_{d=0}^2 \sum_{e=0}^2 c_{\alpha} \cdot X_1^a \cdot X_2^b \cdot X_3^c \cdot X_4^d \cdot X_5^e \quad (10)$$

The polynomial terms comprise products made up of  $n$ -combinations ( $n = 0, 1, \dots, 5$ ) taken from a set of ten elements containing variables  $X_1, X_2, X_3, X_4, X_5$  and their squares, such that the exponent of each variable is less than or equal to two.

Polynomial (10) presents an acceptable compromise between computational cost and accuracy. Experiments using higher-order polynomials did not lead to improved accuracy; on the contrary, they led to severe oscillations and required too many support points. It may be noted that similar numerical experiences are described in the article [77] in connection with Response surface methods.

Polynomial (10) has  $3^5 = 243$  terms with 243 constants  $c_{\alpha}$  where  $\alpha = 81a + 27b + 9c + 3d + e$ . Constants  $c_{\alpha}$  are calculated using the least square method with 400 support points, which are generated using the Latin Hypercube Sampling method (LHS) [78,79]. The first 300 support points are generated for random variables  $X_1, X_2, \dots, X_5$  in Table 2. The other 100 support points are generated for random variables  $t_2, f_y, E, e_0, res$  in Table 1 with settings for the absolute value for each random realization  $e_0$ . The combination 300 + 100 is a compromise ensuring that a sufficient number of the 300 support points (Table 2) are found in a sufficiently wide input space (a sufficiently wide domain for approximation) and another 100 support points (Table 1) increase the density of the input space with the highest frequency of "real" observations of initial imperfections. As a result, the inputs of polynomial (10) can contain up to 500 thousand LHS simulations of the random initial imperfections shown in Table 1. This is a statistically sufficient number of runs for our study, which would have been impossible to perform by direct calculation of the above-mentioned non-linear FE model in real time. The process of generating support points using the 300 + 100 method was chosen empirically according to [80].

## 6. Statistical analysis of the load-carrying capacity

The objective of the statistical analysis is to determine the mean value, standard deviation and design quantiles of the load-carrying capacity. The statistical analysis is performed for two million runs of the LHS method using the inputs listed in Table 1. The set containing two million runs is compiled by combining four sets, each containing 500 thousand runs. Random realizations  $e_0$  are considered using their absolute values. This process ensures that all simulated runs are found within the domain of polynomial (10).

Table 3  
2<sup>5</sup> design performed for standard deviations.

Symbol	Characteristic	Standard deviation Low-level (–)	Standard deviation High-level (+)
$t_2$	Flange thickness	$c_L \cdot 0.518$ mm	$c_H \cdot 0.518$ mm
$f_y$	Yield strength	$c_L \cdot 16.8$ MPa	$c_H \cdot 16.8$ MPa
$E$	Modulus of elasticity	$c_L \cdot 10$ GPa	$c_H \cdot 10$ GPa
$e_0$	Initial imperfection	$c_L \cdot L/1960$	$c_H \cdot L/1960$
$res$	Residual stress	$c_L \cdot 18$ MPa	$c_H \cdot 18$ MPa

The statistical analysis procedure can be described as follows: The non-dimensional slenderness of the beam  $\bar{\lambda}_{LT}$  is selected (e.g.  $\bar{\lambda}_{LT} = 1.0$ ) and the corresponding beam length  $L$  is calculated (e.g.  $L = 2.96$  m), which is also the parameter of the standard deviations in Table 1 and Table 2. The analytical equation is listed in [8]. The curve approximating the analytical relation for  $\bar{\lambda}_{LT} \leq 1.7$  is  $L \approx 2.15\bar{\lambda}_{LT} - 0.75\bar{\lambda}_{LT}^2 + 1.95\bar{\lambda}_{LT}^3 - 0.39\bar{\lambda}_{LT}^4$ . The approximation polynomial (10) is created following the procedure described in the previous chapter. Statistical analysis based on polynomial (10) is performed for the random variables listed in Table 1. An example of the evaluation of the statistical analysis is shown in Fig. 11. The design value of 35.2 kN is evaluated in accordance with [7] for reliability index  $\beta_d = 3.8$  as the 0.1 percentile [11,81]. The 0.1 percentile is evaluated non-parametrically so that two thousand simulation runs lie below the value 35.2 kN, see Fig. 11.

Statistical analysis is performed for additional  $\bar{\lambda}_{LT}$  values. In order to obtain a continuous distribution of the statistical characteristics of the LCC, a step of 0.01 is used for  $\bar{\lambda}_{LT}$ . The results of the statistical analysis after polynomial fitting are depicted in red in Fig. 12. The full lines represent the design values, which are of key importance for reliable design and the assessment of bearing structures. The general case equations are considered the assessment equations of EC3 [8]. The experimentally obtained LCC of the beam should be higher than the design value with a probability of 99.9%. However, this is satisfied only approximately. EC3 [8] does not guarantee sufficient reliability in the design of slender beams, see Fig. 12. The 0.1 percentile values are smaller than the design values evaluated according to EC3 [8] for  $\bar{\lambda}_{LT} > 1.1$ . For high slenderness values, the design value according to EC3 is dangerously close to the mean value, and the mean value dangerously approaches the elastic critical moment  $M_{cr}$  calculated for a beam with nominal characteristics. From a technical perspective, the difference between EC3 and the 0.1 percentile is relatively small for real beams with  $\bar{\lambda}_{LT} < 2$ . The curve of the 0.1 percentile is a smooth curve without a plateau, which differentiates it from the buckling curves in EC3 [8].

Fig. 13 supplements Fig. 12 with the statistical analysis of the LCC of a beam whose residual stress is fixed on the values (i) zero and (ii) 160 MPa. The comparison between (i) and (ii) is noticeably manifested in the interval  $\bar{\lambda}_{LT} \in (0.3, 1.5)$ , see Fig. 13. It may be noted that the values of 0 MPa and 160 MPa were chosen for the purpose of illustrative comparison; however, the most extreme of the recorded experimental residual stress values may be even greater. The most extreme values at the flange tips have even been recorded as being tensile [82].

Another study, shown in Fig. 14, supplements the results in Fig. 12 with a statistical analysis of the LCC of beams whose standard deviation of bow imperfection  $\sigma_{e0}$  is considered to be one-tenth of the value listed in Table 1. The influence of the one-tenth standard deviation of the bow imperfection is observed in the interval  $\bar{\lambda}_{LT} \in (0.2, 1.7)$ , see Fig. 14.

The results in Fig. 13 and Fig. 14 show that the influence of residual stress and bow imperfection on the LCC (mean value and 0.1 percentile) is similar but not identical.

It must be emphasized that the scope of the presented research is limited to beams with an IPN 200 cross-section and cannot be generalized, e.g. to beams with an IPE 200 cross-section.

## 7. Sensitivity analysis results

### 7.1. Sensitivity analysis results based on Spearman's rank-order correlation

SA based on Spearman's rank-order correlation demonstrates the effect of changes in the probability distributions of initial imperfections listed in Table 1 on the probability distribution of the LCC. Spearman's rank-order correlation is the non-parametric version of the Pearson product-moment correlation. Spearman's rank-order correlation coefficient determines the strength and direction of the monotonic (linear or non-linear) relationship between two variables. Fig. 15

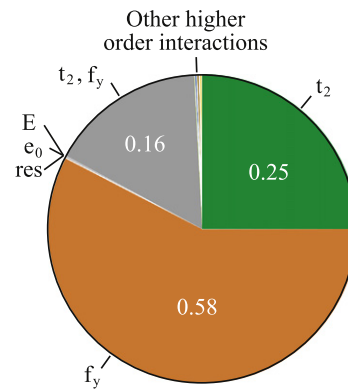


Fig. 16. SAFD for factors in Table 3,  $c_L = 0.01$ ,  $c_H = 1$  and  $\bar{\lambda}_{LT} = 0$ .

shows curves derived using Spearman's rank-order correlation coefficient. Five-hundred thousand LHS runs are used. In order to fulfil the assumption of a monotonic relationship the simulation runs  $e_0$  are considered in absolute values. Imperfections  $f_y$ ,  $t_2$  and  $E$  influence the LCC positively, imperfection  $e_0$  and  $res$  negatively. The influence of  $e_0$  compared to the influence of  $res$  is approximately double and is observed in the double interval  $\bar{\lambda}_{LT}$ , see Fig. 15. The correlation that is absolutely the strongest is related to imperfections  $f_y$ ,  $t_2$ .

The curves derived using Spearman's rank-order correlation coefficient provide a basic understanding of the sensitivity of the LCC to initial imperfections, but cannot evaluate higher interaction effects between the initial imperfections and the LCC [15]. Furthermore, the evaluation of the correlation does not allow the evaluation of the effects of changes in the statistical characteristics of input imperfections on the 0.1 percentile, which is an important design characteristic.

### 7.2. Sensitivity analysis results based on factorial design

Why apply SAFD – sensitivity analysis based on factorial design? Most sensitivity analysis methods study the influence of the random variability of input variables (for which it is assumed that their variability is known) on the random variability of the output variable [15]. However, the design of reliable steel structures is based on design values, which are quantiles. In order to understand how reliably the value of a given quantile is calculated, it is necessary to identify the sources of uncertainty of the input factors and analyse their effects on the design quantile. Major sources of uncertainty could include the standard deviations, mean values and types of pdf of imperfections, which cannot be precisely studied experimentally. A typical example is residual stress, whose statistical characteristics (particularly the standard deviation) and pdf type are still under discussion [13,39]. The question is how to analyse the effect of changes in the standard

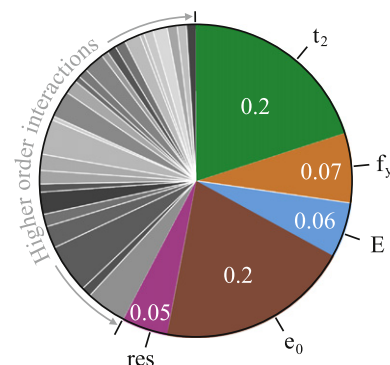


Fig. 17. SAFD for factors in Table 3,  $c_L = 0.01$ ,  $c_H = 1$  and  $\bar{\lambda}_{LT} = 1$ .

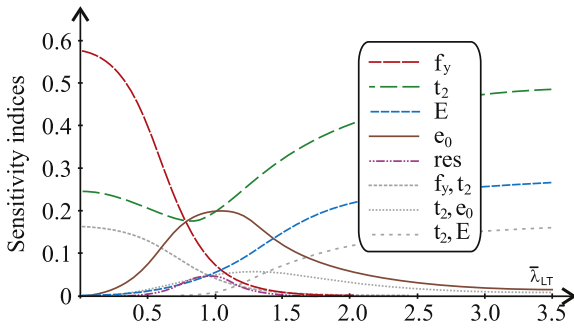


Fig. 18. SAFD for factors in Table 3,  $c_L = 0, c_H = 1$ .

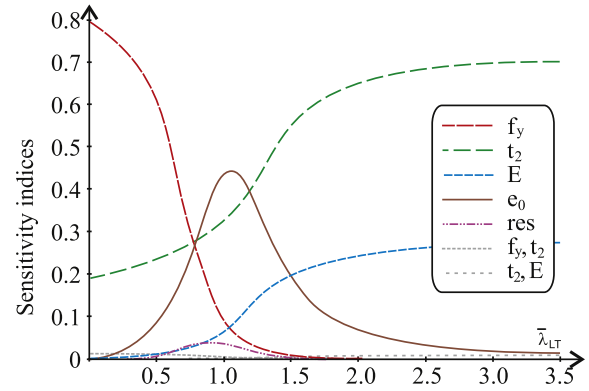


Fig. 20. SAFD for factors in Table 3,  $c_L = 0.49, c_H = 0.51$ .

deviation of an input imperfection (relative to the standard deviations of other imperfections) on the magnitude of  $LCC_{0,1}$ . Such a change can be seen as being purely two-level; it does not burden the study with additional parameters. The results are obtained using SAFD, which evaluates the effects on  $LCC_{0,1}$  of changes in the statistical characteristics of input imperfections.

Five factors are chosen to build the full FD. The factors are the standard deviations of initial imperfections, see Table 3. SAFD examines how the introduction of initial imperfections using deterministic (non-random) values influences the size of the 0.1 percentile. Low-levels (–) are considered to be values very close to zero ( $c_L = 0.01$ ) and high-levels (+) are values from Table 1 ( $c_H = 1$ ). The value  $c_L = 0$  is not considered; this is to prevent analysis taking place on the edge points of the domain of polynomial (10). The pdf types and mean values are the same as in Table 1. The evaluation of  $LCC_{0,1}$  is performed 32 times for all  $2^5$  combinations, see Fig. 10. It is performed using polynomial (10) and 2 million LHS runs for each combination. The outputs of SAFD are the absolute values of sensitivity indices (Eq. (8)), whose sum is normalized to the value of 1. Using the contrast coefficients in Fig. 10, Eq. (8) is used in the form below (Eq. (11)).

$$S_j = \frac{1}{16} \left| \sum_{i=1}^{32} (c_{ij} y_i) \right| \quad (11)$$

Fig. 16 shows the results of SAFD for  $c_L = 0.01, c_H = 1$  and  $\bar{\lambda}_{LT} = 0$ . It can be noted that the results shown in Fig. 16 are the same as for  $c_L = 0$ .  $LCC_{0,1}$  is most influenced by the absence of the random variability of yield strength  $f_y$ , which is the imperfection with the most important main effects. The second most significant main effect is the flange thickness  $t_2$ . The interaction effect of imperfections  $t_2, f_y$  is also significant.

Fig. 17 shows the results of SAFD for  $c_L = 0.01, c_H = 1$  and  $\bar{\lambda}_{LT} = 1$  ( $L = 2.96$  m). The main effect of imperfections  $t_2$  and  $e_0$  has the highest value. The sum of all interaction effects, which is shown in grey in Fig. 17, is relatively significant. The continuous results of

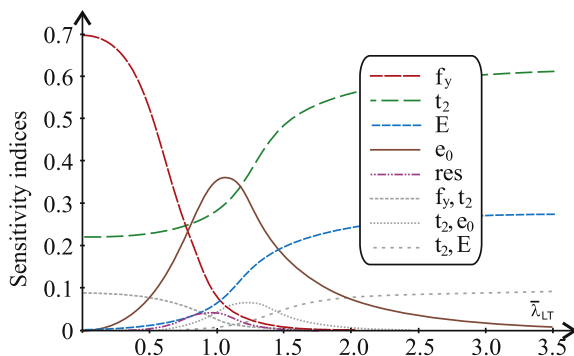


Fig. 19. SAFD for factors in Table 3,  $c_L = 0.3, c_H = 0.7$ .

SAFD for  $c_L = 0.01, c_H = 1$  obtained using the step-by-step method are shown in Fig. 18. Sensitivity indices with very small values are not shown for the sake of clarity.

In further studies, SAFD is evaluated for other settings of  $c_L, c_H$ . Fig. 19 shows the results of SAFD for  $c_L = 0.3, c_H = 0.7$ . Fig. 20 shows the results of SAFD for  $c_L = 0.49, c_H = 0.51$ . The curves of the sensitivity indices in Figs. 18, 19, 20 are approximately similar in shape, but different in size. It is apparent that the values of the sensitivity indices of the first order (main effects) increase and the interaction effects between input factors decrease with decreasing interval size ( $c_L, c_H$ ). The effect on the  $LCC_{0,1}$  value of changes in the standard deviation of the residual stress is not as significant as changes in the standard deviation of the flange thickness or bow imperfection.

In another study, factors are introduced using the mean values of the initial imperfections, see Table 4. Low-levels (–) are the mean values from Table 1 and high-levels (+) are the mean values from Table 1 plus  $c$ -times the standard deviation of the corresponding imperfection, see Table 4. Fig. 21 shows the results of SAFD for  $c = 0.1$ . Fig. 22 shows the results of SAFD for  $c = 0.01$ . The results show the dominant presence of sensitivity indices of the first order; interaction effects are minimal. The results in Fig. 21 and Fig. 22 are practically identical.

### 8. Conclusion

The results of statistical and sensitivity analyses of the LCC of a beam with an IPN 200 cross-section based on a detailed geometric and material non-linear FE model and using SOLID185 finite elements are presented in the article. Using SOLID185 finite elements makes it possible to model the changing flange thickness of the IPN cross-section and to eliminate certain undesirable effects of shell models, such as the small material overlap in the transition between the web and flanges [4]. The problem of material overlap is, however, eliminated at the price of greater (more than three times higher) model processing time. The model's output LCC is approximated using a polynomial in order to permit the use of a high number of LHS runs. The polynomial approximates the input space using five crucial input random imperfections in a manner that retains all non-linear and interaction effects of the non-linear computational model.

Table 4  
2<sup>5</sup> design performed for mean values.

Symbol	Characteristic	Mean value Low-level (–)	Mean value High-level (+)
$t_2$	Flange thickness	11.3 mm	$c \cdot 11.3$ mm
$f_y$	Yield strength	297.3 MPa	297.3 MPa + $c \cdot 16.8$ MPa
$E$	Modulus of elasticity	210 GPa	210 GPa + $c \cdot 10$ GPa
$e_0$	Initial imperfection	0	$c \cdot L/1960$
$res$	Residual stress	90 MPa	90 MPa + $c \cdot 18$ MPa

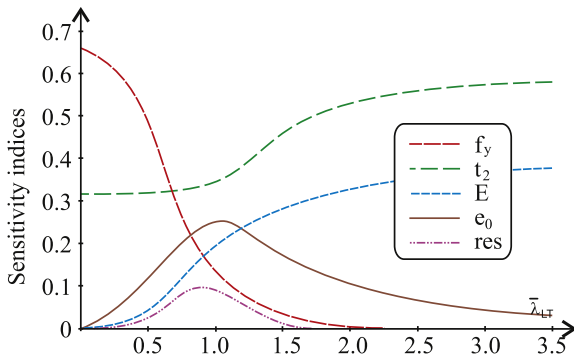


Fig. 21. SAFD for factors in Table 4,  $c = 0.1$ .

The design LCC of EUROCODE 3 is verified via statistical analysis of the LCC, including the calculation of  $LCC_{0.1}$ , which is the 0.1 percentile of the LCC [7]. The results of the statistical analysis show that EUROCODE 3 [8] provides reliable design for  $\bar{\lambda}_{LT} \leq 1.1$ , where  $LCC_{0.1}$  is up to 3% higher than the design LCC according to [8]. On the other hand, the design LCC according to [8] is up to 12% higher (less safe) than the 0.1 percentile for slender beams with  $1.1 < \bar{\lambda}_{LT} \leq 3.5$ . These results confirm the conclusions of the probabilistic reliability analysis [75], according to which the design of very slender beams subjected to bending and solved with consideration given to buckling has a failure probability higher than the optimal target value of  $7.2E-5$  ( $\beta_d = 3.8$ ) [7].

$LCC_{0.1}$  is influenced by the residual stress in the interval  $\bar{\lambda}_{LT} \in (0.3, 1.5)$ , see Fig. 13. This result is obtained by fixing the residual stress on the values zero and 160 MPa and simultaneously keeping the random variability of the other imperfections. A similar (but not identical) effect occurs due to the decrease in the standard deviation of the bow imperfection, see Fig. 14.

Let us compare the results in Fig. 14 with the results of a similar study in [50], which is based on the closed-form analytical elastic solution. The sensitivity of the 0.1 percentile to the bow imperfection is higher in the closed-form analytical elastic solution [50] than in the geometrical and material non-linear FE model presented here. In the study [50] in Fig. 12, setting  $e_0 = 0$  is the limit case, which leads to an LCC value that is equal to (i), the critical elastic moment for slender beams, or (ii), the attainment of yield strength by the extreme fibres

of the cross-section in the case of short beams. The non-linear FE model based on SOLID185 elements used in this paper does not yield such a rapid increase in the LCC for  $e_0 \rightarrow 0$ , and the curves of  $LCC_{0.1}$  vs  $\bar{\lambda}_{LT}$  in Fig. 12 to Fig. 14 retain their shape even for small  $e_0$  values. As a result, the FE model differs from the elastic analytical solution [50], particularly with regard to (i) and (ii).

The main results related to  $LCC_{0.1}$  are obtained by SAFD sensitivity analysis, which describes the influence of inaccuracies in the statistical moments of input variables (the second degree of uncertainty). The statistical moments are (i) standard deviations and (ii) mean values of initial imperfections. Statistical moments (i) and (ii) should be known as accurately as possible. However, the statistical moments of, e.g. residual stress or initial bow imperfection can only be obtained experimentally with limited accuracy [14]. Therefore, the question of how inaccuracies in (i) and (ii) influence  $LCC_{0.1}$  is under investigation.

The main output of SAFD is sensitivity indices, which are plotted in relation to  $\bar{\lambda}_{LT}$ ; see Fig. 18 to Fig. 22. SAFD has shown that the inaccuracies in the residual stress in (i) and (ii) influence the  $LCC_{0.1}$  value in a manner which is relatively very small in comparison to the influence of the inaccuracies caused by the other imperfections in (i) and (ii). The relatively low sensitivity of  $LCC_{0.1}$  to the mean value or standard deviation of the residual stress reduces the uncertainty encountered while introducing the first two statistical moments of the residual stress into the stochastic computational model. The optimistic conclusion of SAFD is also corroborated by the Spearman's rank-order correlations in Fig. 15 and by the Sobol's sensitivity analysis of LCC in [39]. On the other hand, statistical moments (i) and (ii) of the bow imperfection should be paid increased attention, particularly if  $\bar{\lambda}_{LT} \approx 1.0$  (see Fig. 18 to Fig. 20).

The presented SAFD approach provides an alternative to conventional methods of global sensitivity analysis by evaluating the effects of non-random factors of stochastic models on output statistical moments, quantiles or failure probability. SAFD provides information on the calculation conditions for design characteristics which guarantee the safety and reliability of structural design. SAFD can be applied to stochastic models with many input random characteristics and non-random factors which cannot be reliably identified using conventional means and remain an ongoing subject of discussion. This is a common case in numerous research projects in which a stochastic computational model is continuously supplemented by additional random and non-random variables.

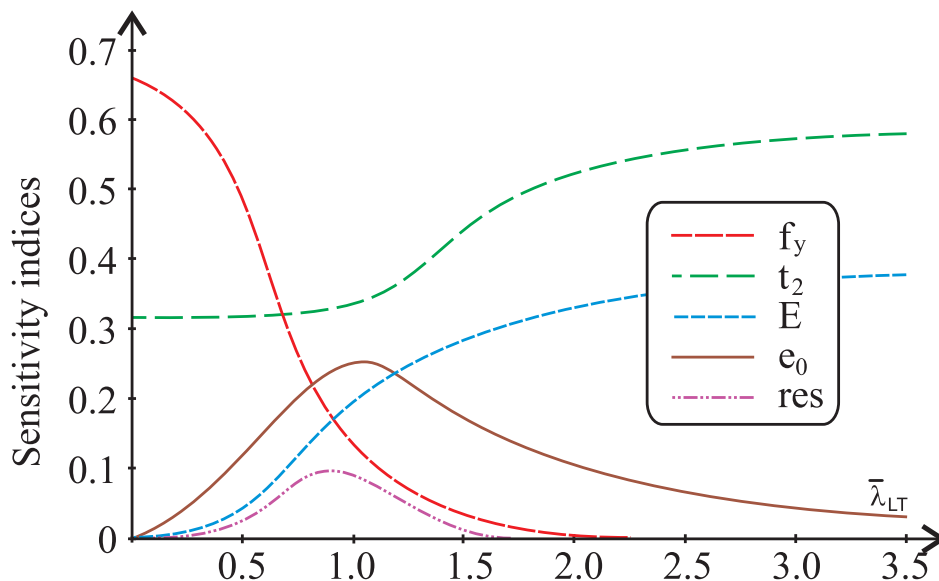


Fig. 22. SAFD for factors in Table 4,  $c = 0.01$ .

The numerical results presented in this article concern only hot-rolled steel beams (IPN 200) under bending. The obtained results and the conclusions formulated based upon them thus cannot be related to other types of hot-rolled or cold-formed members with other types of loading. Future research could focus on the expansion of the studies detailed above to investigate other types of cross-section shape used with hot-rolled imperfect members (I-section, U-section, T-section, etc.) or cold-formed imperfect members loaded not only by bending but also by pressure, or a combination of both. Simultaneously, information needs to be accumulated regarding probabilistic models of initial imperfections, which contribute the most to the lowering of the second degree of uncertainty of stochastic models and their outputs.

## Acknowledgements

The article was prepared within the framework of project No. LO1408 “AdMaS UP”.

## References

- [1] R.D. Ziemian, Guide to Stability Design Criteria for Metal Structures, 6th edition John Wiley & Sons, Inc., 2010
- [2] J.C. Helton, J.D. Johnson, C.J. Sallaberry, C.B. Storlie, Survey of sampling-based methods for uncertainty and sensitivity analysis, *Reliab. Eng. Syst. Saf.* 91 (2006) 1175–1209.
- [3] M. Abambres, M.R. Arruda, Finite element analysis of steel structures – a review of useful guidelines, *Int. J. Struct. Integ.* 7 (4) (2016) 490–515.
- [4] J. Jönsson, T.C. Stan, European column buckling curves and finite element modelling, *J. Constr. Steel Res.* 128 (2017) 136–151.
- [5] G. Sedlacek, C. Müller, The European standard family and its basis, *J. Constr. Steel Res.* 62 (2006) 1047–1059.
- [6] A. Kudzyś, O. Lukoševičienė, The application of a compound model for predicting reliability indices of engineering systems, *Mechanika* 22 (2) (2016) 143–148.
- [7] EN 1990, Eurocode: Basis of structural design, CEN - European committee for standardization, Brussels (Belgium) (2002).
- [8] ENV, 1993-1-1:1992, Eurocode 3: Design of Steel Structures – Part 1.1: General Rules and Rules for Buildings, CEN - European Committee for Standardization, Brussels (Belgium), 1992.
- [9] J. Melcher, Z. Kala, M. Holický, M. Fajkus, L. Rozlívka, Design characteristics of structural steels based on statistical analysis of metallurgical products, *J. Constr. Steel Res.* 60 (3–5) (2004) 795–808.
- [10] J. Szalai, F. Papp, On the probabilistic evaluation of the stability resistance of steel columns and beams, *J. Constr. Steel Res.* 65 (2009) 569–577.
- [11] Z. Kala, J. Melcher, L. Puklický, Material and geometrical characteristics of structural steels based on statistical analysis of metallurgical products, *J. Civ. Eng. Manag.* 15 (3) (2009) 299–307.
- [12] A. Sadowski, J.M. Rotter, T. Reinke, T. Ummenhofer, Statistical analysis of the material properties of selected structural carbon steels, *Struct. Saf.* 53 (2015) 26–35.
- [13] S. Shayan, K.J.R. Rasmussen, H. Zhang, Probabilistic modelling of residual stress in advanced analysis of steel structures, *J. Constr. Steel Res.* 101 (2014) 407–414.
- [14] M. Abambres, W.M. Quach, Residual stresses in steel members: a review of available analytical expressions, *Int. J. Struct. Integ.* 7 (1) (2016) 70–94.
- [15] A. Saltelli, S. Tarantola, F. Campolongo, M. Ratto, *Sensitivity Analysis in Practice: A Guide to Assessing Scientific Models*, John Wiley and Sons, New York, 2004.
- [16] E. Borgonovo, E. Plischke, Sensitivity analysis: a review of recent advances, *Eur. J. Oper. Res.* 248 (3) (2016) 869–887.
- [17] F. Ferretti, A. Saltelli, S. Tarantola, Trends in sensitivity analysis practice in the last decade, *Sci. Total Environ.* 568 (2016) 666–670.
- [18] P. Wei, Z. Lu, J. Song, Variable importance analysis: a comprehensive review, *Reliab. Eng. Syst. Saf.* 142 (2015) 399–432.
- [19] W. Tian, A review of sensitivity analysis methods in building energy analysis, *Renew. Sust. Energ. Rev.* 20 (2013) 411–419.
- [20] W.J.H. Van Groenendaal, J.P.C. Kleijnen, Deterministic versus stochastic sensitivity analysis in investment problems: an environmental case study, *Eur. J. Oper. Res.* 141 (2002) 8–20.
- [21] G. Zagari, G. Zucco, A. Madeo, V. Ungureanu, R. Zinno, D. Dubina, Evaluation of the erosion of critical buckling load of cold-formed steel members in compression based on Koiter asymptotic analysis, *Thin-Walled Struct.* 108 (2016) 193–204.
- [22] Z. Mróz, R.T. Haftka, Design sensitivity analysis of non-linear structures in regular and critical states, *Int. J. Solids Struct.* 31 (15) (1994) 2071–2098.
- [23] C. Szymczak, Sensitivity analysis of thin-walled members, problems and applications, *Thin-Walled Struct.* 41 (2–3) (2003) 271–290.
- [24] M. Koteľko, P. Lis, M. Macdonald, Load capacity probabilistic sensitivity analysis of thin-walled beams, *Thin-Walled Struct.* 115 (2017) 142–153.
- [25] K. Prasad, E.K. Zavadskas, S. Chakraborty, A software prototype for material handling equipment selection for construction sites, *Autom. Constr.* 57 (2015) 120–131.
- [26] J. Antucheviciene, Z. Kala, M. Marzouk, E.R. Vaidogas, Solving civil engineering problems by means of fuzzy and stochastic MCDM methods: current state and future research, *Math. Probl. Eng.* 2015 (2015) 1–16 (Article ID (362579)).
- [27] G. Greegar, C.S. Manohar, Global response sensitivity analysis of uncertain structures, *Struct. Saf.* 58 (2016) 94–104.
- [28] Z. Kala, Global sensitivity analysis in stability problems of steel frame structures, *J. Civ. Eng. Manag.* 22 (3) (2016) 417–424.
- [29] J. Cariboni, D. Gatelli, R. Liska, A. Saltelli, The role of sensitivity analysis in ecological modelling, *Ecol. Model.* 203 (1–2) (2007) 167–182.
- [30] J. Melchers, M. Ahmmed, A fast approximate method for parameter sensitivity estimation in Monte Carlo structural reliability, *Comput. Struct.* 82 (2004) 55–61.
- [31] Z. Lu, S. Song, Z. Yue, J. Wang, Reliability sensitivity method by line sampling, *Struct. Saf.* 30 (6) (2008) 517–532.
- [32] P. Annoni, R. Bruggemann, A. Saltelli, Random and quasi-random designs in variance-based sensitivity analysis for partially ordered sets, *Reliab. Eng. Syst. Saf.* 107 (2012) 184–189.
- [33] A. Glyk, D. Solle, T. Scheper, S. Beutel, Optimization of PEG–salt aqueous two-phase systems by design of experiments, *Chemom. Intell. Lab. Syst.* 149 (2015) 12–21.
- [34] P. Vainiūnas, R. Šalna, D. Šakinis, Probability based design of punching shear resistance of column to slab connections, *J. Civ. Eng. Manag.* 21 (6) (2015) 804–812.
- [35] J. Kim, J.H. Park, T.H. Lee, Sensitivity analysis of steel buildings subjected to column loss, *Eng. Struct.* 33 (2) (2011) 421–432.
- [36] T. Haukaas, M.H. Scott, Shape sensitivities in the reliability analysis of nonlinear frame structures, *Comput. Struct.* 84 (2006) 964–977.
- [37] T. Aven, T.E. Nøkland, On the use of uncertainty importance measures in reliability and risk analysis, *Reliab. Eng. Syst. Saf.* 95 (2) (2010) 127–133.
- [38] B. Möller, U. Reuter, *Uncertainty Forecasting in Engineering*, Springer, 2007.
- [39] Z. Kala, J. Valeš, Global sensitivity analysis of lateral-torsional buckling resistance based on finite element simulations, *Eng. Struct.* 134 (2017) 37–47.
- [40] ANSYS Theory Release 15.1., ANSYS Inc., 2014
- [41] S.P. Timoshenko, J.M. Gere, *Theory of Elastic Stability*, 2nd edition McGraw-Hill, New York, 1961.
- [42] E. Riks, An incremental approach to the solution of snapping and buckling problems, *Int. J. Solids Struct.* 15 (7) (1979) 529–551.
- [43] ENV, 1993-1-5:12006, Eurocode 3: Design of Steel Structures – Part 1.5: Plated Structural Elements, CEN - European committee for Standardization, Brussels (Belgium), 2006.
- [44] A. Taras, R. Greiner, New design curves for lateral-torsional buckling – proposal based on a consistent derivation, *J. Constr. Steel Res.* 66 (2010) 648–663.
- [45] T.T. Nguyen, T.M. Chan, J.T. Mottram, Influence of boundary conditions and geometric imperfections on lateral-torsional buckling resistance of a pultruded FRP I-beam by FEA, *Compos. Struct.* 100 (2013) 233–242.
- [46] A. Agüero, F.J. Pallarés, L. Pallarés, Equivalent geometric imperfection definition in steel structures sensitive to lateral torsional buckling due to bending moment, *Eng. Struct.* 96 (2015) 41–55.
- [47] E. Ghafoori, M. Motavalli, Lateral-torsional buckling of steel I-beams retrofitted by bonded and un-bonded CFRP laminates with different pre-stress levels: experimental and numerical study, *Constr. Build. Mater.* 76 (2015) 194–206.
- [48] P. Panedpojaman, W. Sae-Long, T. Chub-uppakarn, Cellular beam design for resistance to inelastic lateral – torsional buckling, *Thin-Walled Struct.* 99 (2016) 182–194.
- [49] N.S. Trahair, *The Behaviour and Design of Steel Structures*, John Wiley and Sons, New York, 1977.
- [50] Z. Kala, Sensitivity and reliability analyses of lateral-torsional buckling resistance of steel beams, *Arch. Civ. Mech. Eng.* 15 (2015) 1098–1107.
- [51] H. Pasternak, G. Kubieniec, Implementation of longitudinal welding stresses into structural calculation of steel structures, *J. Civ. Eng. Manag.* 22 (1) (2016) 47–55.
- [52] B.W. Young, Residual Stresses in Hot Rolled Members/ABSE reports of the working commissions 1975.
- [53] Ultimate limit state calculation of sway frames with rigid joints/Technical Committee 8 – Structural Stability Technical Working Group 8.2 – System Publication No. 33. European Convention for Constructional Steelwork, 1984.
- [54] A. Kervalishvili, I. Talvik, Influence of residual stress on the stability of steel columns at elevated temperatures, *J. Civ. Eng. Manag.* 23 (2) (2017) 292–299.
- [55] J. Kala, Z. Kala, Residual stresses models for steel rolled profiles - stochastic approach, part 1: imperfections and their consideration in analysis model, *Eng. Mech.* 7 (3) (2000) 219–230 (in Czech).
- [56] Z. Kala, J. Kala, Sensitivity analysis of lateral buckling stability problems of hot-rolled steel beams, *Slovak J. Civ. Eng.* 13 (2) (2005) 9–14.
- [57] A.K. Bhownik, G.Y. Grondin, Limit state design of steel columns reinforced with welded steel plates, *Eng. Struct.* 114 (2016) 48–60.
- [58] J. Valeš, T.C. Stan, FEM modelling of lateral-torsional buckling using shell and solid elements, *Procedia Eng.* 190 (2017) 464–471.
- [59] ABAQUS CAE, v6.13–4, Simulia2014.
- [60] J. Valeš, Z. Kala, J. Martinásek, A. Omishore, FE nonlinear analysis of lateral-torsional buckling resistance, *Int. J. Mech.* 10 (2016) 235–241.
- [61] Z. Kala, J. Vales, J. Martinasek, Inelastic finite element analysis of lateral buckling for beam structures, *Procedia Eng.* 172 (2017) 481–488.
- [62] E.G. Ravandi, R. Rahmnejad, S. Karimi-Nasab, A. Sarrafi, Sensitivity analysis of effective parameters on water curtain performance for crude oil storage in Iranian URC using the 2<sup>k</sup> factorial design and numerical modeling, *Tunn. Undergr. Space Technol.* 58 (2016) 247–256.
- [63] R.A. Fisher, *The Design of Experiments*, Oliver and Boyd, Edinburgh, 1935.
- [64] G.E.P. Box, W.G. Hunter, J.S. Hunter, *Statistics for Experimenters: an Introduction to Design, Data Analysis and Model Building*, John Wiley and Sons, New York, 1978.
- [65] G.E.P. Box, N.R. Draper, *Empirical Model-Building and Response Surfaces*, John Wiley and Sons, New York, 1987.
- [66] J. Antony, *Design of Experiments for Engineers and Scientists*, 1st edition Butterworth-Heinemann, Amsterdam, 2003.

- [67] D.C. Montgomery, Design and Analysis of Experiments, 6th edition John Wiley and Sons, Hoboken, 2013.
- [68] L. Eriksson, E. Johansson, N. Kettaneh-Wold, C. Wikström, S. Wold, Design of Experiments: Principles and Applications, 3rd edition MKS Umetrics AB, Umeå, 2008.
- [69] V. Sethuraman, D. Raghavarao, Balanced 2<sup>n</sup> factorial designs when observations are spatially correlated, *J. Biopharm. Stat.* 19 (2009) 332–344.
- [70] A. Heredia-Langner, E.N. Lored, D.C. Montgomery, A.H. Griffin, Optimization of a bonded leads process using statistically designed experiments, *Robot. Comput. Integr. Manuf.* 16 (2000) 377–382.
- [71] A. Elhalil, H. Tounsadi, R. Elmoubarki, F.Z. Mahjoubi, M. Farnane, M. Sadiq, M. Abdennouri, S. Qourzal, N. Barka, Factorial experimental design for the optimization of catalytic degradation of malachite green dye in aqueous solution by Fenton process, *Water Resour. Ind.* 15 (2016) 41–48.
- [72] Z. Kala, Global interval sensitivity analysis of Hermite probability density function percentiles, *Int. J. Math. Model. Methods Appl. Sci.* 10 (2016) 373–380.
- [73] Z. Kala, Fuzzy sensitivity analysis for reliability assessment of building structures, *AIP Conf. Proc.* 1738 (380007) (2016)<https://doi.org/10.1063/1.4952168>.
- [74] C. Rebelo, N. Lopes, L. Simões da Silva, D. Nethercot, P.M.M. Vila Real, Statistical evaluation of the lateral torsional buckling resistance of steel I-beams, part 1: variability of the Eurocode 3 resistance model, *J. Constr. Steel Res.* 65 (2009) 818–831.
- [75] Z. Kala, Reliability analysis of the lateral torsional buckling resistance and the ultimate limit state of steel beams with random imperfections, *J. Civ. Eng. Manag.* 21 (7) (2015) 902–911.
- [76] G.C. Soares, Uncertainty modelling in plate buckling, *Struct. Saf.* 5 (1988) 17–34.
- [77] G. Bucher, A comparison of approximate response functions in structural reliability analysis, *Probab. Eng. Mech.* 23 (2008) 154–163.
- [78] M.D. McKey, W.J. Conover, R.J. Beckman, A comparison of the three methods of selecting values of input variables in the analysis of output from a computer code, *Technometrics* 1 (2) (1979) 239–245.
- [79] R.C. Iman, W.J. Conover, Small sample sensitivity analysis techniques for computer models with an application to risk assessment, *Commun. Stat. Theory Methods* 9 (17) (1980) 1749–1842.
- [80] Z. Kala, Higher-order approximations methods for global sensitivity analysis of non-linear model outputs, *Int. J. Math. Comput. Simul.* 10 (2016) 260–264.
- [81] Z. Kala, J. Valeš, J. Jönsson, Random fields of initial out of straightness leading to column buckling, *J. Civ. Eng. Manag.* 23 (7) (2017) 902–913.
- [82] P.F. Dux, S. Kitipornchai, Inelastic beam buckling experiments, *J. Constr. Steel Res.* 3 (1) (1983) 3–9.